Journal of Materials Chemistry A

PAPER

View Article Online
View Journal | View Issue

Cite this: J. Mater. Chem. A, 2015, 3, 5409

The co-crystal of TNT/CL-20 leads to decreased sensitivity toward thermal decomposition from first principles based reactive molecular dynamics†

Dezhou Guo,[ab] Qi An,[b] Sergey V. Zybin,[b] William A. Goddard III,*[b] Fenglei Huang[a] and Bin Tang[b]

Received 12th December 2014
Accepted 26th January 2015

DOI: 10.1039/c4ta06858k

www.rsc.org/MaterialsA

To gain an atomistic-level understanding of the experimental observation that the cocrystal TNT/CL-20 leads to decreased sensitivity, we carried out reactive molecular dynamics (RMD) simulations using the ReaxFF reactive force field. We compared the thermal decomposition of the TNT/CL-20 cocrystal with that of pure crystals of TNT and CL-20 and with a simple physical mixture of TNT and CL-20. We find that cocrystal has a lower decomposition rate than CL-20 but higher than TNT, which is consistent with experimental observation. We find that the formation of carbon clusters arising from TNT, a carbon-rich molecule, plays an important role in the thermal decomposition process, explaining the decrease in sensitivity for the cocrystal. At low temperature and in the early stage of chemical reactions under high temperature, the cocrystal releases energy more slowly than the simple mixture of CL-20–TNT. These results confirm the expectation that co-crystallization is an effective way to decrease the sensitivity for energetic materials while retaining high performance.

1. Introduction

Development of new energetic materials with low impact sensitivity and high performance is of great interest for applications in civil constructions, explosives, rocket propellants, and airbag inflators.[1] We consider here a promising engineering strategy for achieving this goal: combining two or more energetic compounds into a "cocrystal" that have solid-state properties distinct from their pure component materials or from just simple physical mixtures.[2] This co-crystallization[3] strategy is also being pursued for pharmaceuticals,[4] optical materials,[5] and semiconducting materials.[6] This strategy provides a new direction to address such sensitivity and performance problems as low density, thermal instability, and high impact and shock sensitivity. In this paper we use first principles based reactive molecular dynamics simulations to predict the change in the initial reaction kinetics for cocrystals and its relation to the decreased sensitivity.

We consider here the 2,4,6,8,10,12-hexanitro-2,4,6,8,10,12-hexaazaisowurtzitane (CL-20) cage structure, which is one of the most promising new energetic materials, because it exhibits high oxygen balance (−10.95%), high density (about 2.0 g cm^{-3}), a large heat of formation (order of 460 KJ mol^{-1}), and superior performance (about 14% higher than HMX).[7] However, CL-20 has not achieved widespread engineering applications because of relative high sensitivity to heat, friction, and shock. Recently, a 1 : 1 molar ratio co-crystal of TNT and CL-20 has been synthesized experimentally[8] that displays greatly reduced sensitivity compared to pure CL-20 while retaining the high performance due to the incorporation of TNT, a relative stable low-power explosive.

We report here an atomistic investigation of how the co-crystal changes the chemical reaction mechanisms at high temperatures, which should be useful for designing other co-crystal combinations with improved properties. Of particular interest is to understand the events occurring at the reactions of these materials.[9]

Various decomposition mechanisms of CL-20 and TNT have been proposed. For example, Nedelko *et al.*[10] proposed a self-acceleration mechanism of CL-20, based on autocatalysis in the pure solid state, which leads to first-order kinetics. Bohn[11] observed auto-catalytically accelerated thermal decomposition of CL-20 and inferred that decomposition is not accompanied by liquefaction. Olexandr *et al.*[12] studied the thermal decomposition of CL-20 using *ab initio* molecular dynamics simulations to predict the chemical behaviour and degradation pathways. Cohen *et al.*[13] investigated thermal decomposition of a single TNT molecule using DFT methods, proposing three possible decomposition paths. Brill and James[14] examined the different thermal decomposition mechanism of TNT under various temperatures and stages.

[a]State Key Laboratory of Explosion Science and Technology, Beijing Institute of Technology, Beijing 100081, People's Republic of China

[b]Materials and Process Simulation Center, California Institute of Technology, 139-74, Pasadena, California 91125, USA. E-mail: wag@wag.caltech.edu

† Electronic supplementary information (ESI) available. See DOI: 10.1039/c4ta06858k

However, little progress has been made in elucidating atomistic details of the complex phenomena occurring in condensed-phase chemistry under extreme conditions of high temperature and high pressure. Indeed, the complexity of the reactions in such systems with numerous intermediates interacting simultaneously might appear to preclude ever obtaining a detailed atomistic understanding of the chemical processes because of the requirement to know the reaction surfaces of thousands of atoms for nanoseconds or longer.

In this paper, we focus on the differences in the initial stages of thermal decomposition among cocrystal, pure crystals, and simple mixtures, as a first step in understanding the complex chemical reaction mechanisms underlying the formation of primary products and aggregates. In order to obtain the different mechanism, we employ the reactive force field (ReaxFF-lg)[15] in a series of reactive molecular dynamics (RMD) simulations.

2. Methodology

2.1. ReaxFF reactive force field

The ReaxFF reactive force field was developed to extend RMD to the study of systems far too large for quantum mechanics (QM), millions of atoms for long periods (many nanoseconds) while retaining nearly the accuracy of QM. The ReaxFF reactive dynamics decompositions have been compared directly with QM for TNT[16] and CH_3NO_2 [17,18] where we find excellent agreement.

Applications with ReaxFF have been reported for many systems (such as RDX, HMX, TATB, and PBX)[15,19–22] involving thermal and shock-induced decompositions at high-temperature and high pressure. These studies have provided valuable information on the atomistic mechanisms of the chemical reactions during decomposition and subsequent reactions under extreme conditions.

2.2. Simulation models and thermal decomposition

The systems studied herein are

- molecular cocrystal of CL-20/TNT,
- pure crystal of CL-20,
- pure crystal of TNT and
- a supercell containing separate grains of CL-20 and TNT.

Among the five temperature-dependent condensed phases of CL-20 (α, β, γ, ξ and δ), we consider here the γ-CL-20 polymorph, which is the most stable phase at room temperature.[23] The initial unit cell structures of cocrystal TNT/CL-20, γ-CL-20 and TNT were taken from Cambridge Crystallographic Data Centre. Each unit cell was then duplicated in all three directions,

- by $(4 \times 2 \times 1)$ for cocrystal TNT/CL-20 to obtain a supercell with 64 CL-20 and 64 TNT molecules;
- by $(2 \times 4 \times 2)$ for γ-CL-20 to provide a supercell with 64 molecules;
- by $(1 \times 2 \times 4)$ for TNT, to provide a supercell with 64 molecules, as shown in Fig. 1.

We first optimized the atomic positions and cell parameters to minimize the potential energy and geometry. Then we carried out isothermal–isobaric (NPT) MD simulations until the system relaxed the internal stresses to zero at room temperature. Here, we used the Nose–Hoover thermostat and barostat (100 fs damping constant for temperature and 8000 fs constant for pressure). The equilibrium densities from ReaxFF were $\rho_0 =$ 1.81 g cm^{-3}, 1.912 g cm^{-3}, 1.71 g cm^{-3} for CL-20/TNT cocrystal, γ-CL-20 and TNT, respectively. These results are in reasonable agreement with the experimental values of 1.91 g cm^{-3}, 1.915 g cm^{-3} and 1.65 g cm^{-3}, respectively. The predicted density, as shown in Table 1, from ReaxFF at ambient condition for the cocrystal is 5.2% below the experiment value, for CL-20 it is 0.5% below experiment, while for TNT it is 3.6% above experiment. This is reasonable since QM calculations on the pure crystal of CL-20 is 6% lower than experiments.[12]

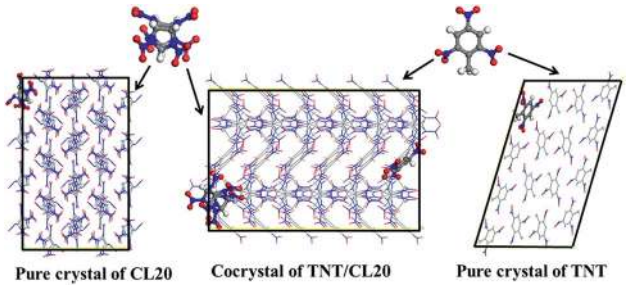

Fig. 1 Structures of the CL-20 and TNT molecules and structures of the CL-20 crystal, TNT/CL-20 cocrystal, and TNT crystal. The cocrystal, composed of a 1 : 1 molar ratio of molecules CL-20 and TNT, leads to a sandwich structure of CL-20 molecule layers separated by TNT ones.

The contributions of the energy components to the stability of the crystals are shown in Table 2. This indicates that for the cocrystal, the binding energy for van der Waals attraction, Coulomb interactions and Hydrogen bond energy are 3.61, −0.60 and -2.3×10^{-4} Kcal g^{-1}; whereas for CL-20 are 3.51, −0.54 and -7.1×10^{-5} Kcal g^{-1}; and for TNT are 3.79, −0.69 and -7.3×10^{-5} Kcal g^{-1}, respectively.

Previous experiments[8] showed that the cocrystal will convert to liquid TNT and either β or γ-CL-20 after heating to a temperature of 409 K. To examine how initial reaction path and energy release rate change for a cooling mixture after reaching the melting point, we constructed the mixed system with two types of amorphous solids and put them separately into two halves of a supercell within a given volume (Fig. 2). We

Table 1 The lattice parameters and density (ρ) of the cocrystal of TNT/CL-20, compared to the pure crystals of CL-20 and TNT

		Parameters of cocrystal			
Comp.	Method	a (Å)	b (Å)	c (Å)	ρ (g cm^{-3})
Cocrystal	ReaxFF-lg	9.98	19.67	24.91	1.81
	Experiment	9.67	19.37	24.69	1.91
CL-20	ReaxFF-lg	13.30	7.88	15.37	1.912
	Experiment	13.23	8.17	14.89	1.915
TNT	ReaxFF-lg	22.10	15.23	5.7	1.71
	Experiment	21.41	15.02	6.09	1.65

Table 2 The contributions of the energy components at ambient conditions to the stability of the crystals

Comp.	Van der Waals attraction (Kcal g^{-1})	Coulomb interactions (Kcal g^{-1})	Hydrogen bond energy (Kcal g^{-1})
Cocrystal	3.61	−0.60	-2.3×10^{-4}
CL-20	3.51	−0.54	-7.1×10^{-5}
TNT	3.79	−0.69	-7.3×10^{-5}

Table 3 The lattice parameters and density (ρ) of the cocrystal of TNT/CL-20, compared to the mixture system

	Parameters of supercell			
Comp.	a (Å)	b (Å)	c (Å)	ρ (g cm^{-3})
Cocrystal	39.92	39.35	24.91	1.81
Mixture	23.65	24.59	68.80	1.77

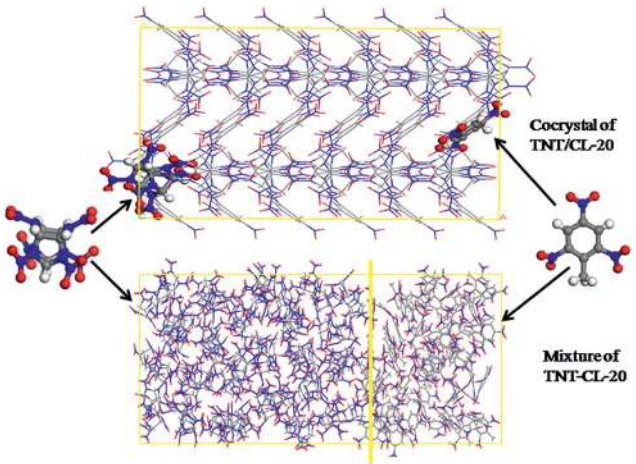

Fig. 2 Comparison of the TNT/CL-20 cocrystal structures and the TNT–CL-20 mixture. The mixture is made by combining a slab of amorphous TNT with a slab of CL-20 molecules each separately into one half side of the supercell, whereas the cocrystal has an ordered sandwich structure.

equilibrated the mixed system by running NPT MD simulation until the internal pressure relaxes to 1 atmosphere at ambient conditions, leading to density of 1.77 g cm^{-3}, which is similar to the cocrystal of 1.81 g cm^{-3}, shown in Table 3.

After equilibration, we performed 100 ps NVT (constant volume, constant temperature, and constant number of atoms) MD simulations on each system at four temperatures: 1200, 1500, 1750 and 2000 K. The integration time step was set to 0.1 fs. In our simulations, we heated the materials quickly (within 3 ps) to the target temperatures to avoid the preceding stage of the shock compression and heating in the detonation wave. To examine the chemical reaction induced energy release process, we also performed NVE (constant volume, constant energy, and constant number of atoms) MD simulations after we heated the materials.

The algorithm for molecule recognition in the species analysis uses the connection table and bond orders calculated by the BondFrag analysis for ReaxFF-lg at each step (the bond order values ranging from 0 to 1 were tabulated in Table S1 in the ESI†). We analysed the molecular components and their compositions every 40 fs. These data were employed to provide detailed information on initial chemical reactions during the decomposition process.

3. Results and discussions

3.1. Thermal decomposition

3.1.1. Potential energy and kinetic rates. Fig. 3 shows the evolution of the potential energy for various systems at temperatures 1500 and 1750 K as a function of time (other temperature situations are shown in Fig. S1 in the ESI†). No obvious changes of potential energy were observed in the TNT system in our simulations. For both CL-20 and the cocrystal, as the temperature increases, the total potential energy increases initially in the induction (endothermic) stage of the

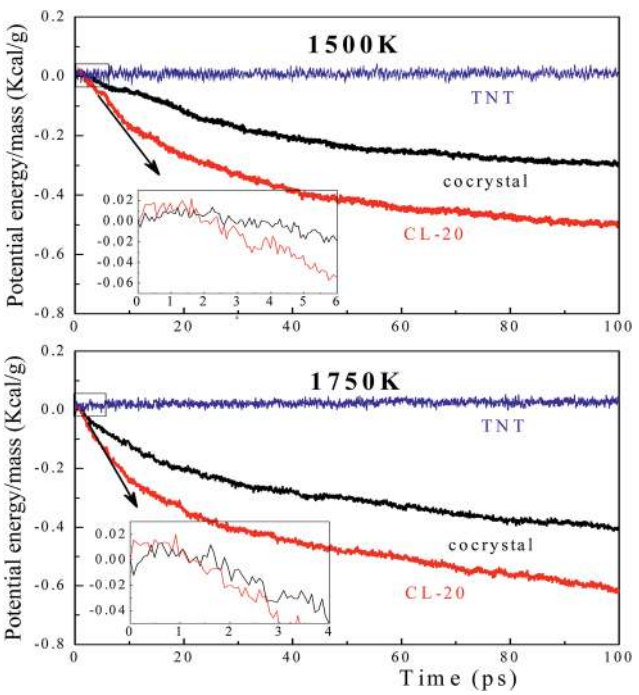

Fig. 3 Evolution of potential energy in the NVT MD simulations of CL-20, cocrystal and TNT. The initial potential energy is set to zero as a reference. For CL-20 and the cocrystal, the rate of potential energy decrease depends strongly on the temperature, whereas TNT does not react significantly under the conditions studied here. At each temperature, the energy release rate of CL-20 is faster than that of cocrystal, which is much faster than TNT.

Table 4 The induction time and reaction rates of cocrystal and CL-20 during various temperatures

	Temperature (K)	1200	1500	1750	2000
Cocrystal	Induction time (ps)	5.2	2.3	1.5	0.8
	Inverse reaction rates (ps)	1155	241	96	52
CL-20	Induction time (ps)	3.4	1.5	0.8	0.4
	Inverse reaction rates (ps)	1957	359	121	61

decomposition due to the endothermic NO_2 dissociation. Then the potential energy decreases after the transition to the energy-releasing stage due to secondary reactions releasing energy from exothermic formation of stable product molecules. This transition happens earlier with increased temperatures.

The reaction rates and induction time, defined as the time at which the potential energy peaks due to initiation of exothermic chemical reactions, are reported in Table 4.

Compared with the pure CL-20 crystal system, the TNT/CL-20 cocrystal shows an induction time 1.5 to 2 times longer and an energy releasing rate 1.2 to 1.7 times lower. This is because the CL-20 molecules in the cocrystal (TNT/CL-20) are surrounded by relatively stable TNT molecules, which isolate the sensitive CL-20 molecules to have less chance to interact with other CL-20 molecules for further chemical reactions.

Our RMD simulations yield kinetic rates of energy-releasing reactions for temperatures between 1200 and 2000 K. Fig. 4 displays reaction rates derived from the potential energy decrease at the exothermic step as a function of inverse temperature. We fit these data using the transition state theory for a first-order reaction rate constant

$$k = \frac{k_B T}{h} e^{\frac{\Delta S^\dagger}{R}} e^{-\frac{\Delta H^\dagger}{RT}} \quad (1)$$

where $\Delta S^\dagger$ is effective activation entropy. Using the transition state theory, we predict that the activation entropy is $\Delta S^\dagger$ = 53.3 cal (mol^{-1} K^{-1}) for cocrystal and 72.0 cal (mol^{-1} K^{-1}) for CL-20.

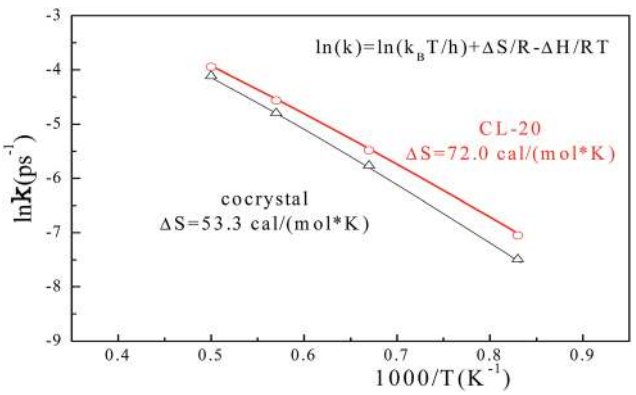

Fig. 4 Reaction rates for cocrystal TNT/CL-20 and pure crystal CL-20 *vs.* inverse temperature (1000/T). The calculated effective activation entropy of chemical reactions is 53.3 cal (mol^{-1} K^{-1}) for cocrystal and 72.0 cal (mol^{-1} K^{-1}) for CL-20.

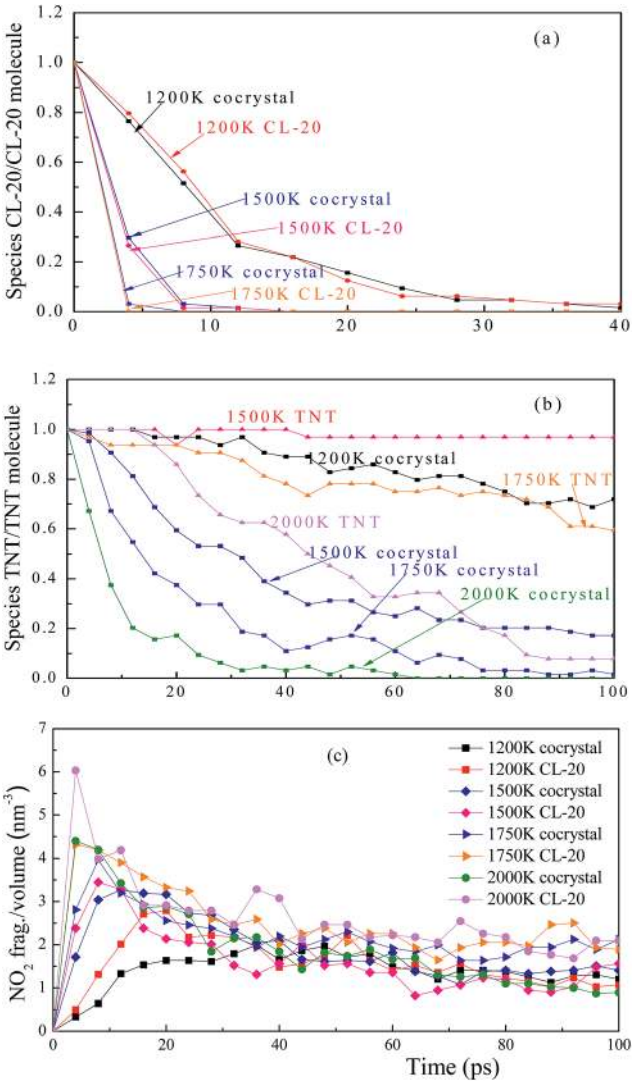

Fig. 5 (a) The number of CL-20 molecules remaining as a function of time during MD-NVT simulations. (b) The number of TNT molecules remaining as a function of time during MD-NVT simulations. (c) Number of free NO_2 molecules as a function of time. This shows that CL-20 molecules in the cocrystal and CL-20 systems have a similar decomposition rate; however, a faster dissociation rate of TNT molecules is observed in the cocrystal than for pure TNT. The production and disappearance of NO_2 fragments is similar for the cocrystals and the parent CL-20 system.

3.1.2. Degree of decomposition. To evaluate the degree of the decomposition of molecules in each system, we count the number of CL-20 and TNT molecules, and the number of dissociated NO_2 molecules, as plotted in Fig. 5.

Fig. 5 shows that the rate of CL-20 decomposition, which increases quickly with temperature and is similar for the co-crystal and pure crystal. However, the TNT decomposition rate increases dramatically for the cocrystal. For instance, for 1500 K at 100 ps, the remaining number of TNT molecules is 18.75% for the cocrystal, and 98.44% for pure TNT. This is because the decomposition of CL-20 molecules, releases energy while forming small active initial or secondary fragments in the co-crystal that can increase the reactivity of the TNT.

For each temperature, CL-20 molecules decompose very quickly compared with TNT molecules, because the energy barrier for C–N bond fission in TNT is higher than N–N bond in CL-20.[24] Moreover, the rupture of the N–NO_2 bond dominates the initial steps for CL-20 dissociation.[25] This result agrees with previous QM[12] and experiment studies on CL-20 reaction pathways.[26]

The evolution of the dissociated NO_2 molecules for the co-crystal in Fig. 5 agrees with that for the parent CL-20 system. With the temperature increase, the rate of NO_2 formation rises quickly in each system. The NO_2 concentration in the pure CL-20 system reaches a higher limit than for the cocrystal system, indicating that pure CL-20 has more intense chemical reactions. In addition, the number of NO_2 molecules in the cocrystal decreases quickly at later time (10–50 ps) at high temperature, because more secondary reactions occur, resulting in rapid consumption of NO_2 molecules and a faster production of stable reaction products, such as N_2, H_2O, and CO_2.

3.1.3. Species analysis. Fig. 6 shows the detailed species analysis of the cocrystal and CL-20 pure crystal at temperatures 1200 and 1750 K. For clarity, only components with relatively high abundance are shown in this figure (other temperature situations are shown in Fig. S2 in the ESI†).

We detected the formation of several key products and intermediates of CL-20 decomposition, such as NO_2, HONO, NO, OH, H_2O, N_2, N_2O, and CO_2, all of which are also observed experimentally.[26–28] Fig. 6 also shows the changes in products for two different materials at various temperatures. In particular, the primary dominant decomposition products, NO_2, are produced faster and in larger quantities at higher temperatures. We found few HONO produced at the early stage in the CL-20 decomposition process, indicating that NO_2 fission dominates initially, followed by ring-breaking. We did find HONO to be formed during the later stages of the reaction probably from NO_2 abstracting a hydrogen atom from other free radical and intermediates. Under such extreme conditions, the HONO molecule is not stable, dissociating rapidly into NO and OH radicals.

These results show that NO_2 fission dominates the early stages of thermal decomposition for CL-20, which differs from the observations in RDX[29]/HMX[30] where both HONO formation and NO_2 fission are competing mechanisms during the initial decomposition.

At high temperature 1750 K, we found that 58.5% fewer CO_2 molecules were formed in the cocrystal system than in pure CL-20 at 100 ps, despite the cocrystal having 5.5 per nm^3 more carbon atoms than CL-20. This is because the decomposition of TNT molecules leads to formation of copious amount of large molecular clusters dominated by carbon atoms, leading to carbon-poor gaseous products.

We found that the formation of final products, H_2O and N_2, as shown in Fig. 7, begins shortly after the initial dissociation of NO_2, with the population of these final products at 100 ps increasing dramatically with temperature, thereby increasing the energy release. These final products in CL-20 appear earlier than in the cocrystal. This indicates that pure CL-20 leads to faster chemical reaction than the cocrystal. This is because the cocrystal system has sensitive CL-20 molecules surrounded by insensitive TNT molecules, which decrease the chance of fragments from decomposition of one CL-20 molecule to contact another CL-20, reducing of the rate of further complex chemical reactions. In addition, for the cocrystal more H_2O fragments

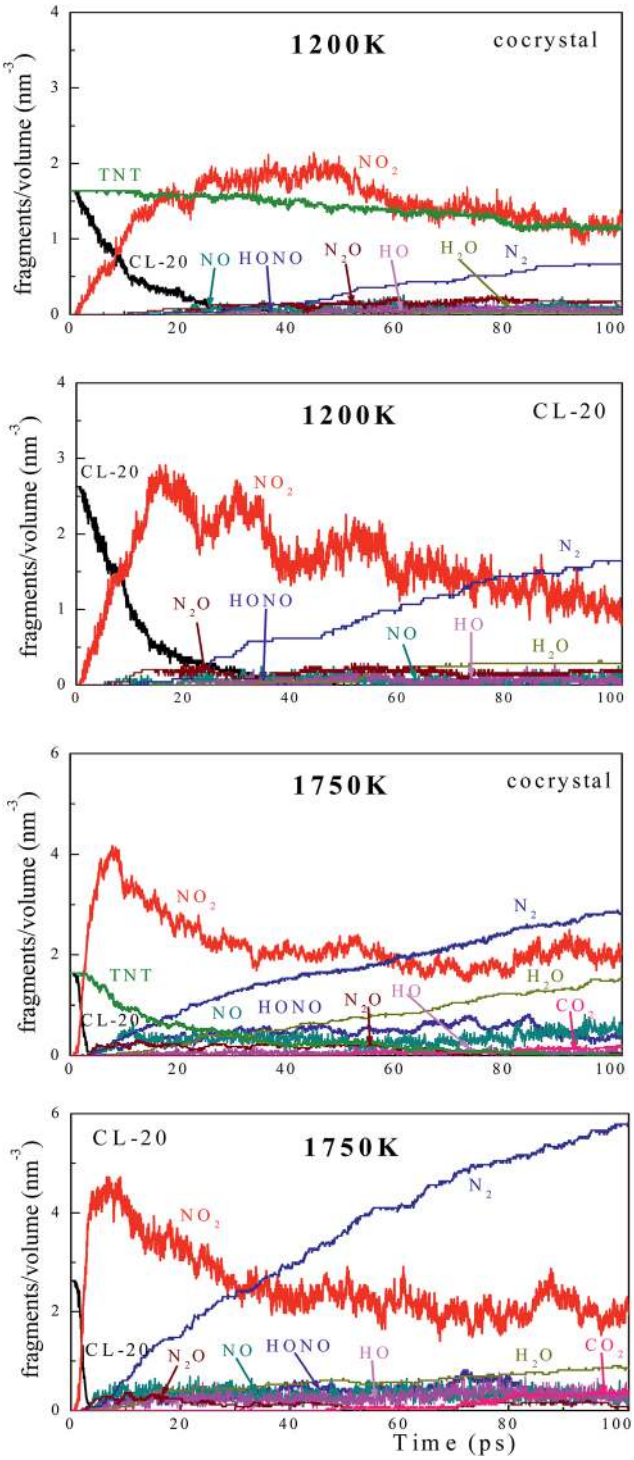

Fig. 6 Evolution of intermediate and secondary products of cocrystal and CL-20 during NVT MD simulation. Chemical reactions occur more intensely in CL-20 than in the cocrystal at each temperature. NO_2 is the dominant product in the early stage of CL-20 dissociation.

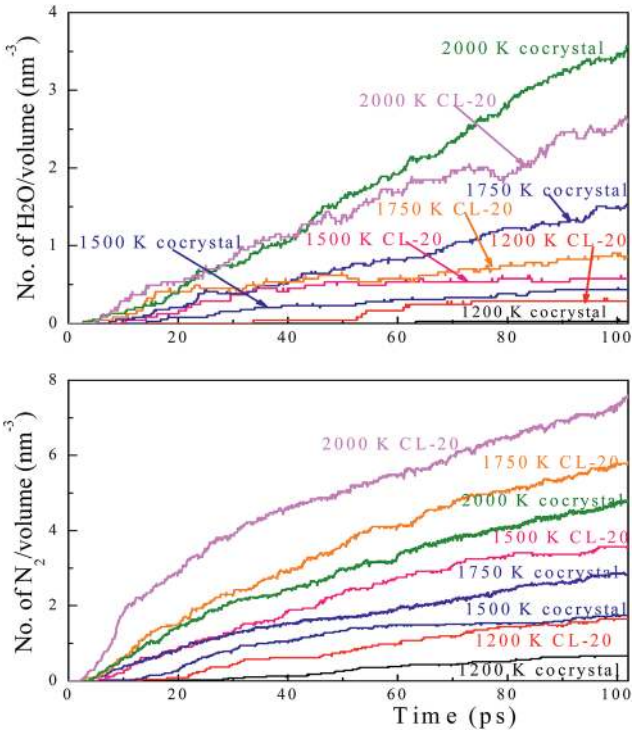

Fig. 7 The number of final products H_2O and N_2 fragments during MD-NVT simulations. These final products were produced earlier in CL-20 than the cocrystal during the decomposition process, indicating more intense chemical reactions in CL-20 system.

were observed at the late stage of reactions under high temperature than for CL-20 because of the participation of TNT molecules.

TNT molecules start to decompose slowly at high temperature, as shown in Fig. 8. The important products and intermediates observed experimentally,[31] such as NO_2, HONO, NO, OH, H_2O, N_2, and CO_2, were observed in the simulations. In particular, at 2000 K, both OH and NO_2 fragments were observed at almost the same time of 10 ps, indicating a different decomposition mechanism for TNT compared with CL-20.

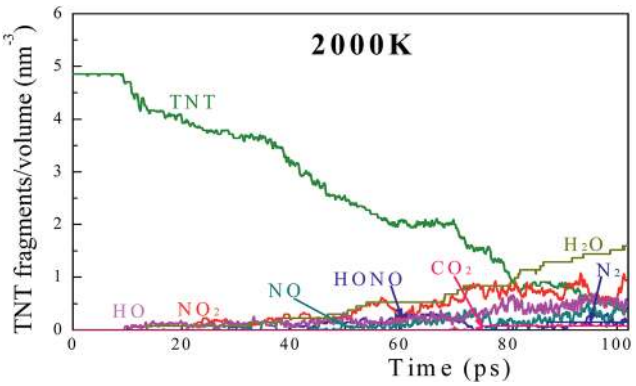

Fig. 8 Time evolution of chemical products of TNT under 2000 K. The slow dissociation rate indicates that TNT has a different decomposition mechanism than CL-20.

Unlike nitramines with the easily broken N–N bond, for TNT both hydrogen bond breaking and C–N bond breaking are likely initial chemical reaction steps, leading to more H_2O fragments formed in the later stage of simulations.[32] These results also help explain the observation that more water molecules were produced in the later stages of the simulations at higher temperatures (1750 and 2000 K).

3.1.4. Carbon-rich clusters. Experiments have shown that carbon clusters can be formed in the detonation process of carbon-rich explosives.[33] This has been confirmed by ReaxFF reactive dynamics simulations comparing HMX with TATB, which find that TATB leads to early formation of carbon clusters containing extensive amounts of N and O that slowly decompose to form stable N_2 and H_2O products while leaving large C clusters.[34] Since the TNT of our cocrystal contains carbon rich benzene rings, we might expect the co-crystal to form carbon rich clusters just as in TATB. If so these carbon clusters might slow down the time for the cocrystal to complete the reactions to form the final dissociation products. Kinetic mechanisms have been developed to characterize the formation of such clusters at the front of the detonation wave and their influence on the properties of the reaction zone.[35–37]

To examine the cluster formation kinetics, we classified the carbon clusters with more than 8 carbons into three types: carbon clusters with eight to twelve carbon atoms, thirteen to seventeen carbon atoms, and more than eighteen carbon atoms.

Fig. 9 shows the time evolution of the three types of carbon clusters in the cocrystal and CL-20 system for temperatures of 1200 and 1750 K (other temperature situations are listed in Fig. S3 in the ESI†). In the CL-20 crystals, the vast majority of carbon clusters are small clusters (C_8–C_{12}) during all simulation times. However, for the cocrystal, we observe many larger

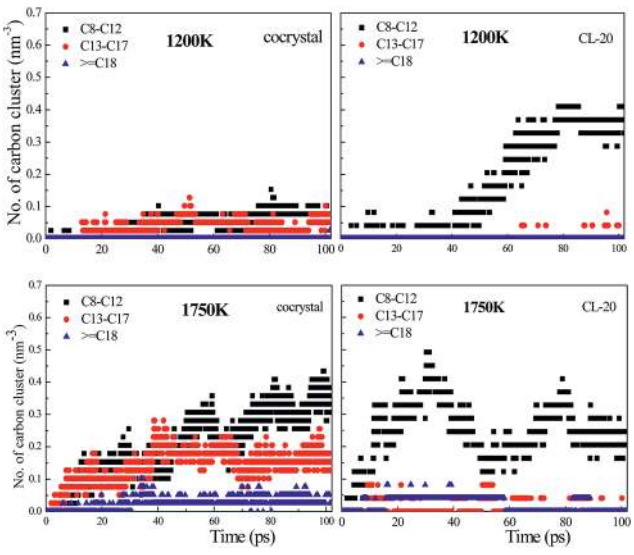

Fig. 9 Time evolution of three types of carbon cluster formed during decomposition for cocrystal and CL-20. More and bigger carbon-rich aggregates are observed in the cocrystal than for CL-20, leading to a slower chemical reaction process.

carbon-reach aggregates (C_{13}–C_{17} with larger than C_{18}). For the low temperature of 1200 K, there are still many more big clusters in the cocrystal even though CL-20 produces more small carbon clusters in CL-20 because of more intense chemical reactions.

As the simulation temperature increases, the number of the big clusters increases in both systems, but the cocrystal leads to formation of much larger carbon-rich aggregates than CL-20. For instance, at the high temperature of 1750 K, the cocrystal leads to an average value of 0.036 per nm^3 of carbon clusters larger than C_{18} and of 0.16 per nm^3 of C_{13}–C_{17} aggregates during the last 40 ps, but CL-20 form only 0.009 per nm^3 and 0.006 per nm^3 clusters, respectively. In addition, we found that any clusters formed in CL-20 are unstable and quickly decompose soon after initiation of secondary reactions.

Our results show that the formation of carbonaceous clusters in the cocrystal begins before complete decomposition of TNT molecules. These clusters slowly release oxygen and nitrogen, producing additional secondary products while transforming into clusters with increased carbon content instead of forming directly the gaseous detonation products of CO_2 or CO that is assumed in common continuum models.[36] We expect that the cluster formation process substantially affects the condensed-phase kinetics of energy-releasing reactions in carbon-rich explosives. These phenomena are consistent with the difference between HMX and TATB carbon cluster formation.[34]

3.2. Stability of carbon clusters after expansion

To examine the evolution of the carbon-rich clusters after expansion of the reaction products into a free volume, we applied the "linear expansion" procedure using variable-volume MD simulation without thermostat: system volume V_0 is linearly increased (with fractional atom coordinates being scaled to the new periodic box) at each time step until it reaches $8V_0$.[34]

We started from the final state of system obtained after 100 ps NVT-MD simulation at 2000 K and expand each cell dimension gradually for 10 ps. After expansion, we fixed the volume and run NVE simulations for 20 ps to examine the dissociation of clusters.

The simulations show that many reactions occur within the initial one ps for the cocrystal and two ps for CL-20 as the clusters decompose, resulting in a decrease in the potential energy. Furthermore, clusters in CL-20 dissociate easily, leading to more decreased potential energy than cocrystal. Since we pump external energy into the system (because the rescaling of atom coordinates during cell expansion imposes an external stretch on the each bond), the potential energy, total energy, and system temperature increases continuously after 1 ps for cocrystal and 2 ps for CL-20, as shown in Fig. 10.

Fig. 11 shows the changes of the three types of clusters during expansion and the next NVE simulations. For CL-20 system, we can't find any big clusters and only a few six to twelve clusters, which decompose quickly in the expansion simulation and finally disappear within 5 ps of NVE simulation. In contrast, more and bigger clusters form in the cocrystal, which then dissociate very slowly in relatively stable configurations over the whole 30 ps of simulation. These carbon clusters play an important role in the thermo chemical reactions, so that the cocrystal has a lower energy release rate and forms fewer final products over our time scale.

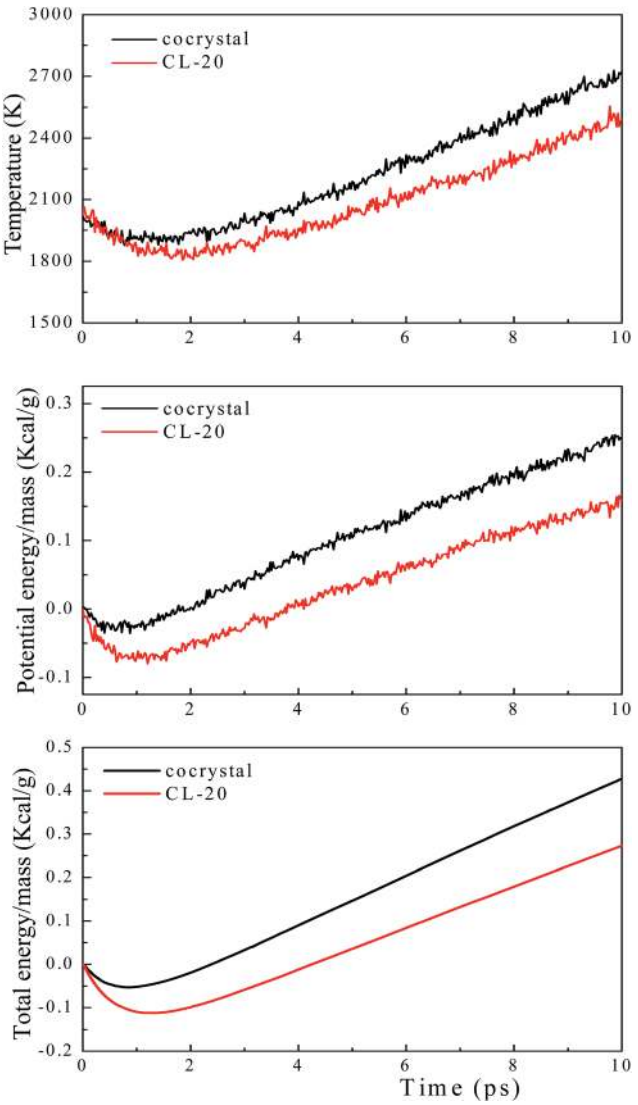

Fig. 10 Time evolution of temperature, potential energy, and total energy for 10 ps variable-volume MD simulations.

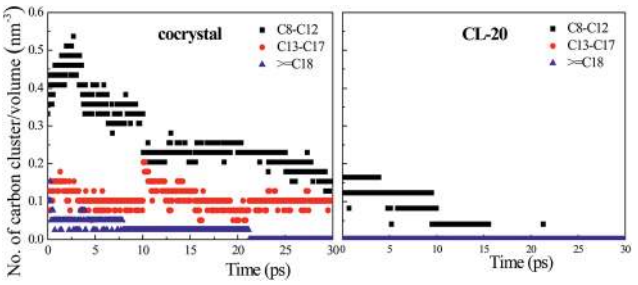

Fig. 11 Time evaluation of three types of carbon clusters during expansion and the next NVE simulations.

These results are in agreement with detonation experiments, which observed the formation of ultrafine diamonds, graphite, and amorphous carbon in post detonation soot from TNT, TNT/RDX, TNT/HMX, TNT/TATB, and other pure and composite explosives.[38]

3.3. Energy release process from chemical reactions

To examine the evolving chemical reaction processes including the role of potential energy release with increasing temperature and product formation, we do not want to use the constant temperature NVT dynamics. Instead we carried out NVE simulations to allow the temperature to adjust to reaction dynamics. The time evolution of potential energy (E_p) directly reflects energy changes along reaction dynamics. Fig. 12(a) and (b) shows that the E_p and temperature changes of pure CL-20, TNT and the cocrystal systems during the NVE simulation with initial temperature of 1500 K (other temperature situations are shown in Fig. S4–S6 in the ESI†).

For a specific initial temperature, the CL-20 system has a fast drop in potential energy and rapid increase of temperature whereas these changes are moderate for the cocrystal. However, TNT molecules alone do not react under these conditions, resulting in no change of potential energy or temperature. Furthermore, the potential energy of CL-20 drops more rapidly than that of the cocrystal until 50 ps. The fast decomposition of NVE results agree with the autocatalytically accelerated thermal decomposition of CL-20, whose cage structure offers opportunities for easy and rapid secondary reactions, leading to efficient energy release capability of CL-20.[39] In addition, there is a fast drop of energy with quick temperature increase and followed by a rise of potential energy in CL-20 system during the NVE simulation.

For both two systems, the NO_2 products, first increase significantly due to CL-20 decomposition, and then decrease gradually after 10 ps due to redox reactions, which in turn form further products, leading to a gradually decreasing of potential energy, as shown in Fig. 12(c) and (d). The CO_2 and N_2 releases cause more rapid potential energy drop than NO_2 dissociation, which leads to an obvious slope change of potential energy and temperature for CL-20 during the NVE simulation. For instance, the potential energy drops sharply from 35 to 50 ps because of the exponentially increasing of N_2 and CO_2. N_2, H_2O and CO_2 molecules appear from about ~5 ps and increase to their maximum number at ~50 ps for CL-20.

The CL-20 system decomposes faster than the cocrystal, leading to increased amounts of final products. For example, compared with the $4N_2$, $2.6H_2O$ and $0.5CO_2$ per nm^3 in cocrystal at 60 ps, we found more than $12N_2$, $3H_2O$ and $7CO_2$ per unit volume final products in CL-20.

For CL-20, the product profiles indicate that most endothermic reactions were completed within 50 ps. Indeed, the evolution of reaction products is consistent with the potential energy release and temperature rise. From 50 to 60 ps, the amounts of H_2O molecules are in a slightly downward trend, but at the same time, OH increases. This indicates that some water molecules were further decomposed above 4000 K,

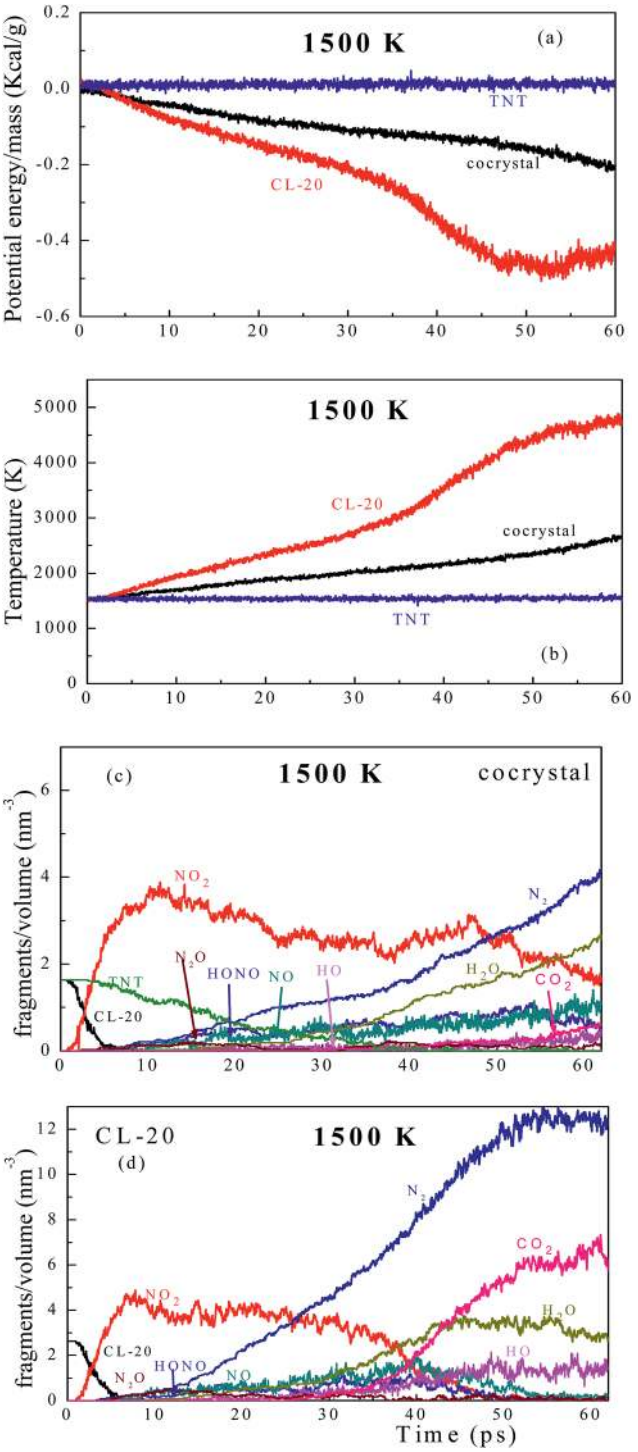

Fig. 12 Normalized potential energy and temperature as a function of time in the NVE MD with an initial temperature $T = 1500$ K. The initial potential energy is set to zero as a reference.

leading to the potential energy increase. The water dissociation was also found in the first-principles molecular dynamics study of PETN[40] and NTO,[41] where the number of OH increases as the temperature goes above 3000 K. Consequently, the reactive OH radicals could be involved in subsequent reactions to play roles of catalysts to drive high temperature dynamics further.

Similarly, we counted the number of three types of carbon clusters in each system under various temperatures to get information of thermal expansion as shown in Fig. 13. Larger and more carbon aggregates, which slow energy release in chemical reactions, were observed in the cocrystal system, playing significant roles in slowing down the chemical reaction process.

3.4. Comparison between the cocrystal and physical mixed systems

3.4.1. Potential energy. To examine the effects of changing sensitivity in the cocrystal, we compare the thermal decomposition of the cocrystal with the physically mixed system. NVT-MD simulations were carried out to examine the thermal decomposition of the TNT–CL-20 mixed system for the same set of temperatures (from 1200 to 2000 K).

Fig. 14 displays the evolution of the potential energy per unit mass (gram) produced by two systems at various temperatures. The decreasing rate of potential energy for each system increases monotonically with the temperature. However, the energy release processes between these two systems are different. For instance, at low temperature 1200 K, the mixture's potential energy change is 16.4% larger than the cocrystal at the end of 100 ps. The reason is that at low temperature, the CL-20 molecules decompose slower in the cocrystal structure than in the mixed structure. This is because that the sandwich arrangement of the cocrystal system makes CL-20 layers isolate by TNT layers. As a result, the initial or secondary fragments dissociated from CL-20 molecules have fewer opportunities to contact with other CL-20 molecules or their products, resulting in less energy release in the early chemical reactions. However, at high temperature 2000 K, although the energy release rate of cocrystal system is lower than mixture system before 20 ps, the potential energy drops faster in cocrystal than mixture in the later process. Now the sandwich arrangement of the cocrystal system makes the TNT molecules decompose faster because of the interactions of the products from CL-20 decomposition. This leads to the potential energy change in mixture 13% less than the cocrystal at 100 ps.

3.4.2. Degree of decomposition. The abundance ratios of undecomposed CL-20 and TNT molecules during the simulations are shown in Fig. 15. As the temperature increases, the decomposition rate of CL-20 molecules was greatly increased so that these molecules in the systems decompose quickly. At the same time, although TNT molecules' decomposition proceeds were much slower than that of CL-20, they also presented an accelerating dissociation rate. In addition, the difference of dissociation rate of TNT of two systems was obvious. For instance, 37.5% TNT molecules in cocrystal have initial chemical reactions at 100 ps compared with 6.25% TNT molecules decompose in mixed system at 1200 K.

3.4.3. Species analysis. Fig. 16 shows a detailed species analysis for the mixture and cocrystal systems at 1200 and 1500 K (other temperature situations are listed in Fig. S7 in the ESI†) for the products with relatively high concentrations, such as NO_2, N_2O, NO, HONO, H_2O, N_2, CO_2 and OH that exhibit substantial dependence on the system temperature.

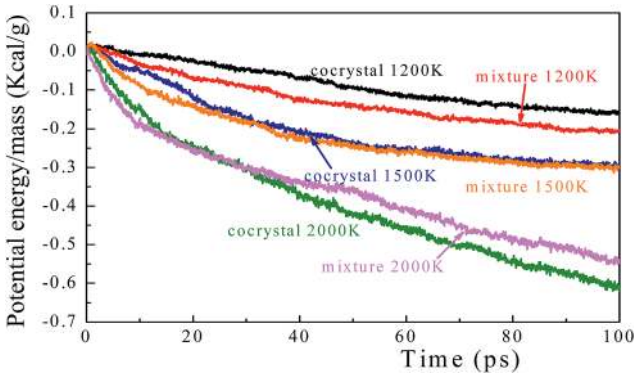

Fig. 14 Evolution of potential energy in MD-NVT simulations of cocrystal and CL-20/TNT mixed system.

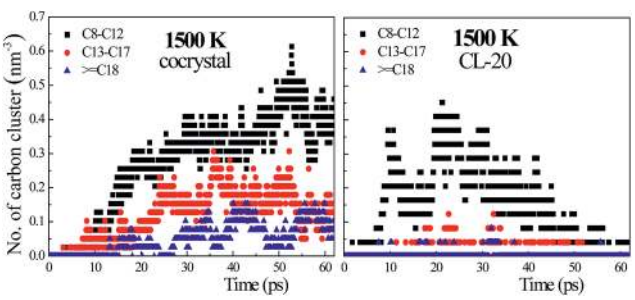

Fig. 13 Time evolution of three types of carbon cluster formed during NVE-MD for cocrystal and CL-20.

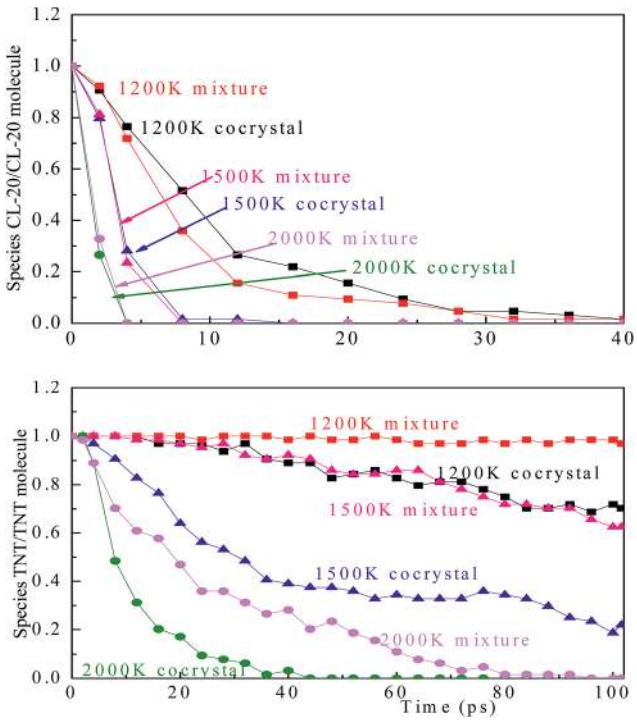

Fig. 15 The number of remaining CL-20 and TNT and dissociated NO_2 molecules during MD-NVT simulations.

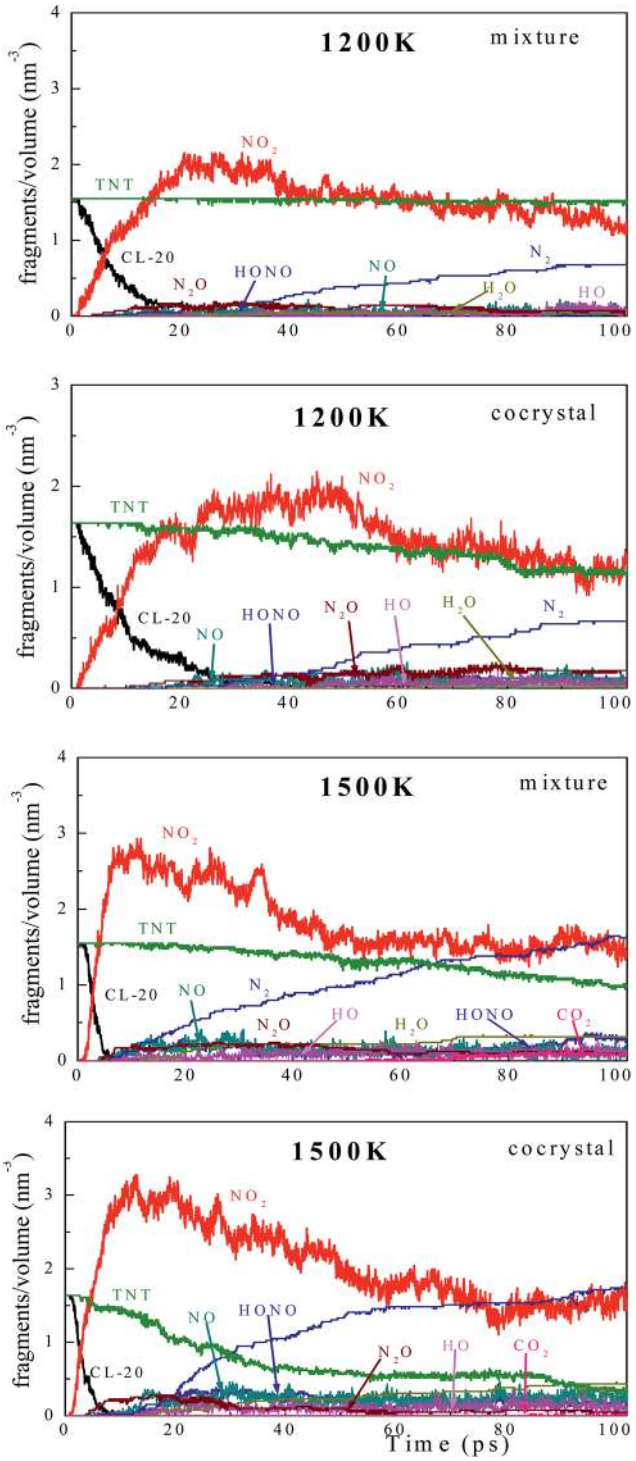

Fig. 16 Evolution of intermediate and secondary products of the mixture and cocrystal systems from NVT MD simulations.

Generally, the species produced for these two systems are quite similar, but the production rates are different. For instance, in the mixture system, the NO_2 production reaches to the maximum value within 50 ps at 1200 K whereas cocrystal system takes 30 ps. At high temperature 1500 K, 64.7% fewer CO_2 fragments are found in the cocrystal due to easier formation of carbon clusters because sensitive CL-20 molecules were surrounded by TNT molecules and the initial or secondary active fragments from CL-20 were trapped into these carbon aggregates. However, TNT molecules have less influence to CL-20 decomposition in mixture system because of less opportunity for these two molecules to contact with each other.

The formation of the final products H_2O and N_2 was observed shortly after NO_2 fragments appeared, and the quantity increasing with the increasing temperature. Both H_2O and N_2 were produced later in the cocrystal system than in mixture system, indicating less intensive reactions in the cocrystal during the early stage because of inhibition of CL-20 dissociation by the nearby TNT molecules. However, for temperatures above 1500 K, more amounts of these final products were attained in cocrystal than in mixtures in the later chemical process, indicating more intensive reactions in the cocrystal systems due to the increased decomposition of TNT molecules.

4. Conclusions

Summary, we report ReaxFF reactive dynamics studies to compare the thermal decomposition processes in cocrystal TNT/CL-20 with pure crystals of TNT and CL-20 and with the simple physical mixtures of these two crystals. We found that the TNT/CL-20 cocrystal releases energy at a lower rate with a higher energy barrier compared to pure crystal of CL-20 and mixture structure, but at a higher reaction rate than pure crystal of TNT.

The rupture of the N–NO_2 bond dominates the initial steps of CL-20 dissociation followed by ring-breaking reaction. The cage structure of CL-20 offers opportunities for easy and rapid secondary reactions, leading to efficient energy release with an autocatalytically accelerated thermal decomposition process. The carbonaceous clusters formed in the decomposition of the cocrystal confine the active fragments, preventing their participation in the secondary reactions. Furthermore, we found that cocrystal releases energy slower than physical mixture of CL-20 and TNT molecules at low temperature and in the early stages of chemical reactions at high temperature.

Our studies demonstrate that ReaxFF MD provides detailed atomistic information that helps to explain the differences between cocrystals and pure crystals or mixtures. This shows that ReaxFF MD captures the fundamental differences in the mechanisms of such systems and illustrates how ReaxFF may be applied to complex chemical phenomena. Developing such detailed chemical kinetics of thermal decomposition reactions could assist in understanding what determine the sensitivity of solid energetic materials to mechanical and thermal shocks, evolution of hot spots, and formation of the reaction zone in the detonation wave. Such thermal and chemical kinetic data is also essential to develop continuum decomposition models that predict the critical conditions for ignition and energy release in hot spots.

Acknowledgements

This work was supported by the U.S. ONR (N00014-09-1-0634). It was also supported by the National Natural Science Foundation of China (grant no. 11172044) and (grant no. 11221202), P. R. China.

Notes and references

1 A. Becuwe and A. Delclos, *Propellants, Explos., Pyrotech.*, 1993, **18**, 1–10.
2 G. P. Stahly, *Cryst. Growth Des.*, 2009, **9**, 4212–4229.
3 A. D. Bond, *CrystEngComm*, 2007, **9**, 833–834.
4 S. G. Fleischman, S. S. Kuduva, J. A. McMahon, B. Moulton, R. D. Bailey Walsh, N. Rodríguez-Hornedo and M. J. Zaworotko, *Cryst. Growth Des.*, 2003, **3**, 909–919.
5 R. Sekiya and R. Kuroda, *Chem. Commun.*, 2011, **47**, 10097–10099.
6 A. N. Sokolov, T. Friščić and L. R. MacGillivray, *J. Am. Chem. Soc.*, 2006, **128**, 2806–2807.
7 R. L. Simpson, P. A. Urtiew, D. L. Ornellas, G. L. Moody, K. J. Scribner and D. M. Hoffman, *Propellants, Explos., Pyrotech.*, 1997, **22**, 249–255.
8 O. Bolton and A. J. Matzger, *Angew. Chem., Int. Ed.*, 2011, **50**, 8960–8963.
9 D. Guo, Q. An, W. A. Goddard III, S. V. Zybin and F. Huang, *J. Phys. Chem. C*, 2014, **118**, 30202–30208.
10 V. V. Nedelko, N. V. Chukanov, A. V. Raevskii, B. L. Korsounskii, T. S. Larikova, O. I. Kolesova and F. Volk, *Propellants, Explos., Pyrotech.*, 2000, **25**, 255–259.
11 M. A. Bohn, *Propellants, Explos., Pyrotech.*, 2002, **27**, 125–135.
12 O. Isayev, L. Gorb, M. Qasim and J. Leszczynski, *J. Phys. Chem. B*, 2008, **112**, 11005–11013.
13 R. Cohen, Y. Zeiri, E. Wurzberg and R. Kosloff, *J. Phys. Chem. A*, 2007, **111**, 11074–11083.
14 T. B. Brill and K. J. James, *Chem. Rev.*, 1993, **93**, 2667–2692.
15 L. Liu, Y. Liu, S. V. Zybin, H. Sun and W. A. Goddard III, *J. Phys. Chem. A*, 2011, **115**, 11016–11022.
16 N. Rom, B. Hirshberg, Y. Zeiri, D. Furman, S. V. Zybin, W. A. Goddard III and R. Kosloff, *J. Phys. Chem. C*, 2013, **117**, 21043–21054.
17 N. Rom, S. V. Zybin, A. C. T. van Duin, W. A. Goddard III, Y. Zeiri, G. Katz and R. Kosloff, *J. Phys. Chem. A*, 2011, **115**, 10181–10202.
18 A. Hervouët, N. Desbiens, E. Bourasseau and J.-B. Maillet, *J. Phys. Chem. B*, 2008, **112**, 5070–5078.
19 A. Strachan, A. C. T. van Duin, D. Chakraborty, S. Dasgupta and W. A. Goddard III, *Phys. Rev. Lett.*, 2003, **91**, 098301.
20 Q. An, S. V. Zybin, W. A. Goddard III, A. Jaramillo-Botero, M. Blanco and S.-N. Luo, *Phys. Rev. B: Condens. Matter Mater. Phys.*, 2011, **84**, 220101.
21 Q. An, W. A. Goddard III, S. V. Zybin, A. Jaramillo-Botero and T. Zhou, *J. Phys. Chem. C*, 2013, **117**, 26551–26561.
22 Q. An, Y. Liu, S. V. Zybin, H. Kim and W. A. Goddard III, *J. Phys. Chem. C*, 2012, **116**, 10198–10206.
23 T. P. Russell, P. J. Miller, G. J. Piermarini and S. Block, *J. Phys. Chem.*, 1993, **97**, 1993–1997.
24 T. B. Brill and K. J. James, *J. Phys. Chem.*, 1993, **97**, 8752–8758.
25 D. G. Patil and T. B. Brill, *Combust. Flame*, 1993, **92**, 456–458.
26 J. K. Rice and T. P. Russell, *Chem. Phys. Lett.*, 1995, **234**, 195–202.
27 J. C. Oxley, A. B. Kooh, R. Szekeres and W. Zheng, *J. Phys. Chem.*, 1994, **98**, 7004–7008.
28 B. L. Korsounskii, V. V. Nedel'ko, N. V. Chukanov, T. S. Larikova and F. Volk, *Russ. Chem. Bull.*, 2000, **49**, 812–818.
29 A. Strachan, E. M. Kober, A. C. T. van Duin, J. Oxgaard and W. A. Goddard III, *J. Chem. Phys.*, 2005, **122**, 054502.
30 T. Zhou and F. Huang, *J. Phys. Chem. B*, 2010, **115**, 278–287.
31 P. S. Makashir and E. M. Kurian, *J. Therm. Anal. Calorim.*, 1999, **55**, 173–185.
32 F. Hosoya, K. Shiino and K. Itabashi, *Propellants, Explos., Pyrotech.*, 1991, **16**, 119–122.
33 E. V. Mironov, E. A. Petrov and A. Y. Korets, *Combust., Explos. Shock Waves*, 2004, **40**, 473–476.
34 L. Zhang, S. V. Zybin, A. C. T. van Duin, S. Dasgupta, W. A. Goddard III and E. M. Kober, *J. Phys. Chem. A*, 2009, **113**, 10619–10640.
35 M. van Thiel and F. H. Ree, *J. Appl. Phys.*, 1987, **62**, 1761–1767.
36 J. A. Viecelli and F. H. Ree, *J. Appl. Phys.*, 2000, **88**, 683–690.
37 J. A. Viecelli, S. Bastea, J. N. Glosli and F. H. Ree, *J. Chem. Phys.*, 2001, **115**, 2730–2736.
38 N. R. Greiner, D. S. Phillips, J. D. Johnson and F. Volk, *Nature*, 1988, **333**, 440–442.
39 M. Geetha, U. R. Nair, D. B. Sarwade, G. M. Gore, S. N. Asthana and H. Singh, *J. Therm. Anal. Calorim.*, 2003, **73**, 913–922.
40 C. J. Wu, L. E. Fried, L. H. Yang, N. Goldman and S. Bastea, *Nat. Chem.*, 2009, **1**, 57–62.
41 Y. Liu, S. V. Zybin, J. Guo, A. C. T. van Duin and W. A. Goddard III, *J. Phys. Chem. B*, 2012, **116**, 14136–14145.